American Mineralogist, Volume 60, pages 1030–1040, 1975

Mica Polytypism: Dissimilarities in the Crystal Structures of Coexisting $1M$ and $2M_1$ Biotite

HIROSHI TAKEDA

Mineralogical Institute, Faculty of Science, University of Tokyo, Hongo, Tokyo 113, Japan

AND MALCOLM ROSS

U.S. Geological Survey, National Center—959, Reston, Virginia 22092

Abstract

Crystal-structure analysis of coexisting $1M$ and $2M_1$ biotite polytypes from a rhyodacite lava flow, Ruiz Peak, New Mexico, shows that the two forms possess essentially identical unit-cell parameters (in the $1M$ setting), bond length averages, and site occupancies and probably, therefore, very similar chemical compositions. The unit layers of the two polytypes, however, are different structually in that the x and y atomic positions of the O3 and O4 oxygens differ in the two forms by an average of 14 standard deviations. The average difference in the relative values of all other atomic positions is one standard deviation. The displacement of O3 and O4 in the $2M_1$ biotite causes a type of deformation not before reported in micas and manifests itself by a relative shifting of the upper and lower triads of octahedral oxygens as a unit along the $\pm b$ directions ($2M_1$ setting). This causes a reduction in symmetry of the $2M_1$ unit-layer from the ideal $C2/m$ as found in the $1M$ polytype, to $C\bar{1}$.

It is postulated that the structural differences between the unit layers of the $1M$ and $2M_1$ biotite polytypes are due to the different atomic and geometric constraints imposed upon the unit layer by the adjacent layers, the latter being in different relative orientations in different polytypes. An origin for biotite polytypism is proposed on the basis of these unit-layer constraints coupled with the mica platelet growth and spiral growth observations of A. Baronnet.

Introduction

In the last decade, many reports have been published on the crystal structure of various mica polytypes. For example, the model structures of $1M$ trioctahedral micas were summarized by Donnay, Donnay, and Takeda (1964) and by Takeda (1971); the unit-layer of $2M_1$ muscovite, refined by Burnham and Radoslovich (1964), was compared with that of the $3T$ form by Güven and Burnham (1967), $1M$ and $2M_1$ brittle micas of different composition were studied by Takéuchi (1964), $1M$ and $2M_2$ lepidolites were studied by Takeda, Haga, and Sadanaga (1971), and a $2O$ brittle mica was examined by Giuseppetti and Tadini (1972). The previous studies of mica polytypes were accomplished on samples from diverse localities having significantly different chemical compositions. It is thus difficult to decide how much the structural differences found between various polytypes are due to chemical differences, differences in temperature and pressure of formation, and differences in the stacking sequence of the unit-layers.[1] Another question is, are the unit layers structurally as well as chemically identical if the mica crystals have different periodic stacking sequences?

The question of possible structural differences between different mica polytypes found in the same rock hand specimen arose during our study of oxybiotites from a rhyodacite lava flow at Ruiz Peak, New Mexico (Ross *et al.*, 1966). Single crystal X-ray study of 42 crystals from this specimen showed that approximately one-third are $1M$ forms, one-third $2M_1$, and one-third more complex polytypes such as the $4M_2$, $8M_8$, and $8Tc_{12}$ forms. The detailed study of the structures of these crystals, however, was postponed, for we did not believe that at that time crystal structure refinements could be done accurately enough to show the very small differences expected between unit layers of different polytypes. The present study of the crystal structures of coexisting $1M$

[1] A mica unit-layer is defined as that layer, approximately 10Å thick, contained in the unit-cell of the $1M$ polytype. Two unit layers occur in the unit cell of the $2M_1$ polytype.

and $2M_1$ polytypes from a single hand specimen of the Ruiz rhyodacite was made during 1972 using the best X-ray diffraction techniques then available. With this study we hope that we may develop a better understanding of the nature and cause of polytypism and polymorphism[2] in complex silicates.

Mineralogy

Specimen Description

The biotite crystals examined in this study occur in a rhyodacite ash flow from the Ruiz Peak area, Valles Mountains, New Mexico. The particular rock sample studied (No. 3149-8) came from the top of the flow and is reddish because of formation of hematite after eruption of the lava. The rock contains abundant phenocrysts of feldspar, biotite, and magnetite and less abundant phenocrysts of augite and orthopyroxene. Apatite is ubiquitous and occurs as inclusions in the biotite. The groundmass is composed mainly of feldspar, glass, and biotite; the latter is much altered to hematite and other products of late stage oxidation (probably sanidine, metastable magnetite, and glass; D. R. Wones, personal communication). The large biotite phenocrysts are often rimmed with hematite, and this phase is also seen in the cleavage cracks. The biotite crystals separated for chemical and crystallographic analysis, however, were nearly free of hematite but still contained apatite inclusions and a small amount of rutile.

The oxidation, which is inferred to have occurred during and after eruption of the lava, affected the biotite crystals in two ways: (1) exposed surfaces of the biotites reacted to form hematite and other breakdown products, and (2) the crystals reequilibrated with respect to the hydrogen fugacity by the reaction, somewhat idealized,

$$KMg_{3-x}Fe^{2+}_{x}(Si_3Al)O_{12}H_2 \rightarrow KMg_{3-x}Fe^{2+}_{x-y}Fe^{3+}_{y}(Si_3Al)O_{12}H_{2-y} + 1/2yH_2\uparrow.$$

This reaction caused the biotite crystals to turn dark reddish brown. Biotite crystals from underlying, unoxidized flows do not show this color and their ferric iron content is much lower.

Chemical Composition

The biotite chemical formulas based on wet chemical and electron microprobe analyses (separates 3149-8F and 3149-8W, respectively) are given in Table 1, columns (1) and (3). Electron probe analyses made on the clear homogeneous areas of five crystals revealed barium—an element missed by the wet chemical analysis—but no calcium. The 0.46 wt percent CaO and 0.34 wt percent P_2O_5 found in the wet analysis is thus due to included apatite. The range of cation content as obtained by microprobe analyses overlaps that given by wet chemical analyses with the exception of higher Mg and Al and lower Fe content. We attribute this difference to chemical differences in the biotite phenocrysts depending upon the time of crystallization from a fractionating melt. The different mineral separates reflect these chemical differences. The biotite crystals studied crystallographically came from separate 3149-8F, and thus we assume that the Mg, Al, and Fe content is closer to that given by the wet chemical analysis. The electron microprobe study did not detect any significant chemical variation within a single biotite crystal.

The oxy-biotite sample under study contains 8.4, 10.6, and 81.0 percent "fluoro", "hydroxy", and "oxy" component, respectively (Table 1, column 1). Of the total "oxy" component 52.8 percent is related to a couple substitution involving oxidation-reduction, that is,

$$Fe^{2+} + OH^- \rightleftharpoons Fe^{3+} + O^{2-} + 1/2H_2.$$

Part or most of this substitution probably occurred as a solid-state reaction during eruption of the lava. Of the (47.2%) remaining "oxy" component, most (42.2%) must be attributed to the incorporation of 0.342 atoms per formula unit of titanium (Table 1) into the crystal structure during crystal growth, charge balance being maintained by increase of the oxyanion content. This coupled substitution may be written

$$K(Mg,Fe)^{2+}_3(Si_3Al)O_{10}(OH)_2 + Ti^{4+} \rightleftharpoons K(Mg,Fe)^{2+}_2Ti(Si_3Al)O_{12} + (Mg,Fe)^{2+} + 2H^+$$

Hydrogenation of Biotite

Hydrogenation of the oxybiotites is easily accomplished by passing hydrogen gas at temperatures of 500° to 700°C over the single crystals. The reac-

[2] We define polytypism as the existence of two or more chemically identical, or nearly identical, phases which have structurally similar unit motifs (unit layers in the case of micas) but which repeat in three-dimensional crystal space in different ways. We define polymorphism as the existence of two or more chemically identical, or nearly identical, phases which do not possess structurally similar unit motifs. Phases such as quartz-coesite and calcite-aragonite can be unambiguously defined as polymorphs whereas substances such as the biotites, zinc sulfides, silicon carbides, and cadmium iodides are generally thought of as showing polytypism.

TABLE 1. Chemical Formulae Based on Wet Chemical Analyses of Separate No. 3149-8F and on Electron Microprobe Analyses of Individual Crystals from Separate No. 3149-8W

Atoms	(1)* Oxybiotite		(2)* Hydrogenated Oxybiotite (700°C)		(3)** Oxybiotite		(Range)
Si	2.841	4.000	2.857	4.000	2.853	4.000	2.794-2.900
Al (IV)	1.159		1.143		1.147		1.222-1.288
Al (VI)	0.163	3.049	0.186	3.112	0.101	3.066	
Ti	0.342		0.344		0.321		0.306-0.338
Mn^{3+}	0.010		0.010		0.018		0.009-0.020
Fe^{2+}	0.855		0.185		0.741		0.742-0.762
Fe	0.013		0.711		0.011		
Mg	1.666		1.676		1.874		1.850-1.906
Ba	0.022	0.957	0.022	0.961	0.020	0.933	0.013-0.022
Na	0.162		0.162		0.157		0.152-0.168
K	0.773		0.777		0.756		0.692-0.802
OH	0.212	12.000	0.711	12.000	-		
F	0.168		0.169		0.138		0.101-0.182
Cl	-		-		0.004		0.002-0.004
O	11.620		11.120		-		

* Atomic ratios based on wet chemical-analysis, chemistry laboratory, U.S. Geological Survey. Summation based on: O+F+OH = 12. BaO from electron microprobe analysis. Fraction 3149-8F. CaO and P_2O_5 are assumed to be in apatite only.

** Atomic ratios based on electron microprobe analysis (average of five analyses on five crystals), analyst - L.B. Wiggins (U.S. Geological Survey). Summation based on 8.000 cations excluding hydrogen. Fraction 3149-8W. Iron is assumed to have the same ferrous - ferric ratios as in (1).

tion is reversible; by passing hot argon gas over the hydrogenated crystals, hydrogen is removed and the crystals revert to their previous structural and chemical state. These oxidation-reduction reactions are of course dependent on the availability of sufficient amounts of an oxidizable metal cation such as iron within the crystal structure. The ferrous and ferric iron content of the Ruiz Peak biotite (separate 3149-8F) before and after hydrogenation at 700°C is given in Table 1, Columns (1) and (2), respectively.

Of particular interest from a crystal-structural standpoint is the possible effect of polytypism on the exact configuration of the unit-layer within the $1M$ and $2M_1$ forms and also the effect of the loss or addition of hydrogen on the structure of the unit layer. With this in mind, the present paper examines in detail the crystal structures of the hydrogenated $1M$ and $2M_1$ polytypes. In a later study we plan to take these same two crystals, remove the hydrogen, and redetermine the crystal structures. Unit-cell dimensions of $1M$ and $2M_1$ oxybiotites before and after hydrogenation at 700°C are given in Table 2. Note the increase in the thickness of the unit-layer of 0.09 Å after hydrogenation. Also, in the same table the unit-cell dimensions of the hydrogenated $1M$ and $2M_1$ oxybiotites as measured with a single crystal diffractometer are compared with those of phlogopite and annite.

Structure Determination

The crystals used for structure determination measure 0.23 × 0.27 × 0.05 mm; the calculated densities are 3.05 g/cm³; and the linear absorption coefficients are 26.6 cm^{-1}.

TABLE 2. Crystal Data for Oxybiotites and Hydrogenated Oxybiotites from Rhyodacite No. 3149-8, Ruiz Peak, New Mexico, and for Phlogopite and Annite (Wones, 1963)

		a(Å)	b(Å)	c(Å)	β
		X-ray precession data†			
oxybiotite	(1M)	5.317	9.22	10.09	100.2
	($2M_1$)	5.315	9.22	19.95	95.1
hydrogenated oxybiotite (700°C)					
	(1M)	5.322	9.22	10.18	100.2
	($2M_1$)	5.335	9.22	20.10	94.9
		Single crystal diffractometer data††			
hydrogenated oxybiotite					
observed	(1M)	5.331(2)	9.231(4)	10.173(4)	100.16(3)
ideal	(1M)*	5.331	9.234	10.170	100.06
observed	($2M_1$)	5.329(2)	9.234(3)	20.098(7)	95.09(3)
calculated	(1M)**	5.331	9.231	10.168	100.14
		X-ray powder data (Wones, 1963)††			
phlogopite	(1M)	5.326(6)	9.210(9)	10.311(9)	100.17(15)
annite	(1M)	5.401(10)	9.347(5)	10.297(10)	100.17(15)

†*Error ~0.2%*

††*Error in parentheses*

**Calculation based on the ideal relationships* $a\sqrt{3} = b$ *and* $\beta = \tan^{-1}(3d_{001}/a)$.

***Unit-cell parameters of the unit layer of the* $2M_1$ *biotite in the 1M setting.*

Intensity measurements were made with a Picker-FACS-I computer-controlled four-circle, single-crystal diffractometer, using Mo$K\alpha$ radiation with a graphite monochromator and a scintillation detector. Intensities of 1202 reflections for the 1M form and 3539 reflections for the $2M_1$ form were measured in the 4°–60° 2θ range using ω-2θ scans. Each reflection was scanned through 1.2°, using dispersion factors of the system for α_1 and α_2 separation at a scanning rate of one degree per minute. The background was obtained by counting for 20 seconds at both sides of the peak. Integrated intensities were corrected for Lorentz and polarization effects and were reduced to structure factors $|F_o|$. The absorption correction was made by Burnham's (1966) subroutine with a linear absorption coefficient of 26.6 cm^{-1} for Mo$K\alpha$ radiation. The estimated standard deviation of an observation was computed on the basis of the counting statistics (Burnham *et al,* 1971).

Of the intensities measured, 649 nonequivalent reflections of the 1M biotite, with the indices hkl and $\bar{h}kl$, and 875 reflections of the $2M_1$ biotite, with the indices $h\bar{k}l$ and $\bar{h}\bar{k}l$, were utilized in the final refinements. The space groups $C2/m$ for 1M and $C2/c$ for $2M_1$ were assumed and, on refinement, turned out to be correct.

The full matrix least-squares program, RFINE (Finger, 1969) which includes the provision for site occupancy refinement, was used for the 1M and $2M_1$ biotite crystal structure determinations. The weights used in refinement are $1/\sigma(Fo)^2$, where $\sigma(Fo)$ is the standard deviation of $|Fo|$. The atomic-scattering factors used with RFINE were taken from Cromer and Mann (1968), the oxygen atoms being considered half-ionized (O^{1-}), and all cations completely ionized. Anomalous dispersion corrections were made by using the coefficients of Cromer (1965).

Least-squares refinement of the 1M structure was initiated by using atomic coordinates of a 1M phlogopite (Joswig, 1972). The trial structure model of the $2M_1$ form was derived from the atomic coordinates of the above 1M phlogopite using a program (TWMC) written for the HITAC 5020E computer (Takeda *et al,* 1971). The hydrogen atoms were not included in these refinements. The following cations were fixed during refinement: K + Na in the interlayer sites, Si + Al^{IV} distributed equally over the tetrahedral sites, and Ti + Al^{VI} + Mn distributed equally over the octahedral sites. The relative amount of Fe + Mg in the two octahedral sites was allowed to vary during refinement. During the site refinement, the occupancy factor of Fe in the $M2$ site was derived from the total amount of Fe in the chemical formula, less that in $M1$. The occupancy of Mg in $M1$ and $M2$ is fixed by the value (1-Ti-Al^{VI}-Mn-Fe) for each of these sites.

In the last stages of refinement, reflections for which $|Fo| < 15$ and $||Fo| - |Fc||/\sigma(Fo) > 5$ were rejected. After six cycles of refinement, during which the scale factor, the atomic coordinates, and the anisotropic temperature factors βij were varied, no further change of parameters took place. The observed and calculated structure factors for the 1M and $2M_1$ polytypes are listed in Tables 3a and 3b, respectively.[3] The final conventional unweighted residuals for structural parameters given in Tables 4 and 5 are $R = 0.044$ for 649 observable reflections of the 1M form and $R = 0.056$ for 875 reflections for the $2M_1$ form.

The various bond lengths (Tables 6, 7, 8), selected bond angles (Table 9), and associated standard deviations were computed from the atomic positions given in Table 5. The variance-covariance matrices (Finger, 1969) of the refinements and the standard deviations of the unit-cell parameters were used for these computations. The observed 1M coordinates are compared in Table 5a with the observed $2M_1$ coordinates in the 1M setting. The latter coordinates are those of the unit layer of the $2M_1$ polytype in the crystallographic orientation of the 1M form and are derived by a matrix rotation of 120° about c^* of coordinates of atoms in a $2M_1$ unit layer (Table 5b) and then translation of the origin to that of the 1M polytype.

Comparison of Structures

Chemical Similarity

The similarity of the unit-cell dimensions and bond lengths of the 1M and $2M_1$ crystals indicate that the crystals are very close in chemical composition. In Table 2 the measured unit-cell dimensions of the 1M form are compared with the calculated unit-cell dimensions of the $2M_1$ polytype in the 1M setting. The agreement between these two sets of unit-cell dimensions is within one standard deviation for all four parameters. Likewise, the mean tetrahedral, the octahedral, and the inner and outer sets of potassium-oxygen bond lengths are essentially identical for both structure types. The comparative values for average bond lengths (Tables 6, 7, 8) for the 1M

[3] To obtain a copy of Table 3a and 3b, order document AM-75-008 from the Business Office, Mineralogical Society of America, 1909 K Street, N.W., Washington, D.C. 20006. Please remit $1.00 for the microfiche.

TABLE 4. Site Occupancy Factors for Coexisting Biotites after Hydrogenation at 700°C*

	M1	M2**
	1*M* Polytype	
Mg	0.537	0.546
Fe	0.290	0.281
Ti + Mn + Al	0.173	0.173
	$2M_1$ Polytype	
Mg	0.568	0.531
Fe	0.259	0.296
Ti + Mn + Al	0.173	0.173

**During least-squares refinement, tetrahedral sites were fixed at Si=0.71, Al=0.29 and the interlayer site at Na=0.22, K=0.78. Total cations in M1+M2 are normalized to 3.000 atoms per formula unit with Mg=1.630, Fe=0.852, and Ti+Mn+Al=0.519. Amount of Ti+Mn+Al in each site is fixed at 0.173. The values for M1+M2 differ slightly from that given in Table 1, column (2) after normalization to 3.000 (viz. Mg=1.617, Fe=0.864, and Ti+Mn+Al=0.521).*

***The occupancy of Mg in M2 is derived by 0.826-0.5x (occupancy of Mg in M1). Error in octahedral occupancies with regard to Mg and Fe may be as large as 10% considering the possible errors in the chemical analyses.*

TABLE 5a. Atomic Coordinates of the Hydrogenated 1*M* and $2M_1$ Biotites from Ruiz Peak, New Mexico*

Atom**	(Form)	x	y	z
M1	(1M)	0	0	0.5
M1	($2M_1$)	0.0002	0.0002	0.5
M2	(1M)	0	0.3392(1)	0.5
M2	($2M_1$)	0.0002	0.3398	0.5
K	(1M)	0	0.5	0
K	($2M_1$)	0	0.5	0
T	(1M)	0.0745(2)	0.1671(1)	0.2242(1)
T1	($2M_1$)	0.0742	0.1673	0.2240
T2	($2M_1$)	0.0741	0.1670	0.2240
01	(1M)	0.0165(7)	0	0.1674(4)
011	($2M_1$)	0.0168	0.0005	0.1676
02	(1M)	0.3240(5)	0.2310(3)	0.1660(3)
021	($2M_1$)	0.3241	0.2300	0.1656
022	($2M_1$)	0.3253	0.2303	0.1668
03	(1M)	0.1310(4)	0.1684(3)	0.3906(2)
031	($2M_1$)	0.1179	0.1733	0.3910
032	($2M_1$)	0.1173	0.1639	0.3906
04	(1M)	0.1312(6)	0.5	0.3985(3)
04	($2M_1$)	0.1180	0.4957	0.3984

* Both forms are listed in the 1M setting to facilitate comparison. The atomic coordinates for the $2M_1$ polytype in the $2M_1$ setting are given in Table 5b.

** Standard deviations for the 1M forms are given in parentheses; those of the $2M_1$ form are listed in Table 5b.

TABLE 5b. Atomic Coordinates of the Hydrogenated Ruiz Peak $2M_1$ Biotite in the $2M_1$ Setting

Atom*	x	y	z
M1	0.75	0.25	0.0
M2	0.2406(3)	0.0802(2)	-0.00004(8)
K	0.0	0.0840(3)	0.25
T1	0.4621(3)	0.2498(2)	0.13798(9)
T2	0.9635(3)	0.4169(2)	0.13799(9)
011	0.7410(8)	0.3140(5)	0.1662(3)
021	0.2430(8)	0.3532(5)	0.1672(3)
022	0.4337(8)	0.0840(5)	0.1666(2)
031	0.4314(7)	0.2406(5)	0.0545(2)
032	0.9375(7)	0.4090(6)	0.0547(2)
04	0.9348(7)	0.0739(5)	0.0508(2)

* Standard deviations are given in parentheses and are expressed in units of last digit stated.

and $2M_1$ forms, respectively, are: tetrahedral (1.659, 1.659 Å), octahedral-*M*1 (2.086, 2.086), octahedral-*M*2 (2.068, 2.067), inner K–O (2.972, 2.972), and outer K–O (3.318, 3.321). The site occupancy factors (Table 4) are also in good agreement for the two polytypes even though the errors are large.

The tetrahedral rotation angle, α, which reflects the degree of deformation of the oxygen ring from hexagonal to ditrigonal symmetry, is 7.61° in the 1*M* form and 7.63° in the $2M_1$ form (Table 9), these values being identical within the accuracy of the refinements. This similarity of rotation angles is expected if the composition of the octahedral and

TABLE 5c. Equivalent Isotropic Temperature Factors *B* and Anisotropic Temperature Factors* $\beta ij \times 10^4$ of Ruiz Peak Biotites

Atom	B	β_{11}	β_{22}	β_{33}	β_{12}	β_{13}	β_{23}
			1M biotite				
M1	1.17(4)	85(5)	19(2)	50(2)	0	23(2)	0
M2	1.17(4)	64(3)	33(1)	41(1)	0	12(1)	0
K	2.29(4)	180(7)	53(2)	79(2)	0	28(3)	0
T	0.75(2)	55(3)	12.7(9)	30.9(8)	0(1)	13(1)	-0.5(9)
01	1.46(6)	172(13)	24(4)	41(4)	0	13(6)	0
02	1.59(5)	115(8)	44(3)	50(3)	-17(4)	17(4)	-6(2)
03	0.99(4)	74(7)	18(2)	33(2)	3(4)	15(3)	0(2)
04	1.03(5)	79(11)	28(4)	31(3)	0	8(5)	0
			$2M_1$ biotite				
M1	0.85(4)	55(7)	25(2)	6.9(6)	0	3(1)	0
M2	1.05(3)	110(5)	26(2)	6.3(3)	20(4)	2(1)	2(1)
K	2.21(4)	182(8)	65(3)	14.6(7)	0	3(2)	0
T1	0.70(3)	52(5)	23(2)	4.7(4)	3(3)	1(1)	1(1)
T2	0.71(2)	53(5)	22(2)	5.0(4)	-6(3)	2(1)	-2(1)
011	1.54(8)	136(17)	54(6)	8(1)	-19(8)	0(4)	1(2)
021	1.53(8)	108(16)	60(6)	8(1)	25(8)	0(4)	-2(2)
022	1.48(7)	181(16)	38(5)	7(1)	3(9)	4(3)	-0(3)
031	0.57(6)	47(12)	7(4)	6(1)	1(7)	3(3)	4(3)
032	0.69(6)	70(12)	14(4)	5(1)	11(8)	2(3)	5(3)
04	0.80(6)	88(13)	11(4)	6(1)	9(8)	0(3)	-0(3)

* βij is in the expression

$$\exp-(\beta_{11}\underline{h}^2 + \beta_{22}\underline{k}^2 + \beta_{33}\underline{\ell}^2 + \beta_{23}2\underline{k}\underline{\ell} + \beta_{13}2\underline{\ell}\underline{h} + \beta_{12}2\underline{h}\underline{k}).$$

TABLE 6. Bond Lengths for Tetrahedral Sites of Ruiz Peak Biotites

1M biotite		$2M_1$ biotite			
Bond	Length (Å)	Bond	Length (Å)	Bond	Length (Å)
T-O1	1.657(2)	T1-O11	1.649(4)	T2-O11	1.659(4)
T-O2	1.655(3)	T1-O21	1.656(4)	T2-O21	1.656(4)
T-O2′	1.657(3)	T1-O22	1.644(5)	T2-O22	1.662(5)
T-O3	1.667(3)	T1-O31	1.675(4)	T2-O32	1.674(4)
Mean	1.659	Mean	1.656	Mean	1.663
			(Mean 1.659)		
O1-O2	2.686(3)	O11-O21	2.682(6)	O11-O21	2.695(6)
O1-O2′	2.691(3)	O11-O22	2.679(6)	O11-O22	2.700(6)
O2-O2	2.688(1)	O21-O22	2.679(6)	O21-O22	2.699(6)
Mean	2.688	Mean	2.680	Mean	2.698
O3-O1	2.731(4)	O31-O11	2.751(6)	O32-O11	2.702(6)
O3-O2′	2.728(4)	O31-O21	2.761(6)	O32-O21	2.716(6)
O3-O2′	2.728(3)	O31-O22	2.673(6)	O32-O22	2.779(6)
Mean	2.729	Mean	2.728	Mean	2.732

TABLE 7. Bond Lengths for Octahedral Sites of Ruiz Peak Biotites

1M biotite		$2M_1$ biotite	
Bond	Length (Å)	Bond	Length (Å)
	M1 Octahedron		
M1-O3	2.102(2)x4	M1-O32	2.034(4)x2
		M1-O31	2.104(4)x2
M1-O4	2.053(3)x2	M1-O4	2.120(4)x2
Mean	2.086	Mean	2.086
	(Shared edges)		
O3-O3	2.828(5)x2	O31-O32	2.730(6)x2
O3-O4	2.769(4)x4	O32-O4	2.770(5)x2
		O31-O4	2.867(7)x2
Mean	2.789	Mean	2.789
	(Unshared edges)		
O3-O3	3.109(5)x2	O31-O32	3.110(5)x2
O3-O4	3.098(4)x4	O31-O4	3.102(5)x2
		O32-O4	3.097(5)x2
Mean	3.102	Mean	3.103
	M2 Octahedron		
M2-O3	2.118(3)x2	M2-O31	2.054(5)
		M2-O32	2.124(4)
M2-O3′	2.083(2)x2	M2-O31′	2.146(4)
		M2-O32′	2.147(5)
M2-O4	2.004(3)x2	M2-O4	1.934(5)
		M2-O4′	1.999(4)
Mean	2.068	Mean	2.067
	(Shared edges)		
O3-O3	2.799(5)x2	O31-O31′	2.792(7)
		O32-O32′	2.895(8)
O3-O3′	2.828(5)x1	O31-O32	2.730(6)
O4-O3	2.769(4)x2	O4-O32′	2.770(5)
		O4-O31′	2.867(7)
O4-O4	2.691(7)x1	O4-O4	2.592(8)
Mean	2.776	Mean	2.774
	(Unshared edges)		
O3-O3	3.062(2)x2	O31-O32′	3.064(5)
		O31′-O32	3.059(5)
O4-O3	3.076(4)x2	O4-O32′	3.073(5)
		O4′-O31′	3.075(5)
O4-O3′	3.062(3)x2	O4-O31	3.058(5)
		O4′-O32	3.065(5)
Mean	3.067	Mean	3.066

TABLE 8. Bond Lengths for Interlayer Sites of Ruiz Peak Biotites

1M biotite		$2M_1$ biotite	
Bond	Length (Å)	Bond	Length (Å)
	(inner)		
K-O1	2.971(4)x2	K-O11	2.975(5)x2
K-O2	2.973(3)x4	K-O21	2.971(5)x2
		K-O22	2.971(4)x2
Mean	2.972	Mean	2.972
	(outer)		
K-O1	3.331(4)x2	K-O11	3.329(5)x2
K-O2	3.312(3)x4	K-O21	3.313(5)x2
		K-O22	3.322(4)x2
Mean	3.318	Mean	3.321
	(lateral)		
O1-O2	4.144(4)x4	O11-O11′	4.166(9)
		O11-O22	4.148(6)x2
O2-O2′	4.143(5)x2	O21-O22	4.145(6)x2
		O21-O21′	4.129(9)
Mean	4.144	Mean	4.147
	(basal)		
O1-O2	4.261(4)x4	O11-O21	4.260(6)x2
		O11-O22	4.257(6)x2
O2-O2′	4.265(6)x2	O21-O22	4.261(6)x2
Mean	4.262	Mean	4.259
	(shortest interlayer lengths)		
O1-O1	3.380(7)x4	O11-O21	3.364(6)x4
O2-O2	3.348(5)x2	O22-O22	3.365(8)x2

tetrahedral sheets of each polytype is similar. The tilting of the tetrahedra, resulting in the corrugation of the tetrahedral sheets so characteristic of the $2M_1$ dioctahedral micas, is not pronounced in either of the biotites.

A comparison of the atomic coordinates of the $1M$ structure with those of a unit layer of the $2M_1$ structure in the $1M$ setting reveals a remarkable agreement between all atomic coordinates, except for the x and y values of the octahedral oxygen atoms O3 and O4. For example, the displacement of the x atomic coor-

TABLE 9. Selected Angles for Computing Tetrahedral Rotation Angles α*

1M biotite		$2M_1$ biotite	
Bond	Angle, deg.	Bond	Angle, deg.
O2′-O1′-O2″	104.82(17)x2	O21′-O11′-O22	104.69(20)
O1-O2-O2′	104.63(10)x4	O11-O21-O22	104.71(18)
		O11-O22-O21′	104.76(19)
Mean	104.69	Mean	104.72
O2-O1″-O2″	135.18(19)x2	O21-O11-O22′	135.30(22)
O2-O2′-O1′	135.08(17)x4	O11′-O21′-O22′	135.20(22)
		O11′-O22-O21	135.27(20)
Mean	135.11	Mean	135.26
α	7.61	α	7.63

* $\alpha = |120° - \text{mean angles}| \times 0.5$.

dinate of oxygen atom O32 of the $2M_1$ structure from the x coordinate of O3 of the $1M$ structure is 0.0137, which is 19 times the standard deviation of the O32 x coordinate (0.0007). The average difference in the x and y parameters of the O3 and O4 oxygens in the two crystal structures is 14 standard deviations. The average difference in the relative x, y, and z positions of all other atoms, including z of O3 and O4, is one standard deviation.

Deformation of $2M_1$ Octahedra

Previous crystal structure studies of $2M_1$ micas have shown that displacement of the O3 and O4 oxygen atoms from the ideal octahedral arrangement causes two types of octahedral deformation: (1) flattening of the octahedra along the pseudo $\bar{3}$ axes (common in disordered trioctahedral micas, Donnay *et al*, 1964), and (2) lengthening of the edges shared between $M1$ and $M2$ octahedra containing monovalent ions or vacancies. The latter type of deformation is found in partially ordered lithium-bearing trioctahedral micas (Takeda and Burnham, 1969) and in dioctahedral micas (Radoslovich, 1960).

The octahedra of the $2M_1$ biotite of this study possess a new mode of deformation. A convenient method of depicting this deformation is to project the shared octahedral edges O31–O31 and O32–O4 onto the (001) plane. These projected edges are inclined approximately 6° from the a axis of the $2M_1$ unit cell (Fig. 1). The equivalent octahedral edge projections of the $1M$ biotite are almost exactly parallel to the a axis when viewed in the $2M_1$ setting. In $2M_1$ muscovite, these same projected edges are also almost exactly parallel to a.

The inclination of the projected edges of the octahedra of the $2M_1$ form relative to those of the $1M$ polytype is presented in Figure 4. Note especially the inclination of the O4–O4 and O31–O32 projections with respect to the equivalent projections of the $1M$ octahedra (solid and dashed lines, respectively, Fig. 4). This distortion of the $2M_1$ octahedra is caused by a "sliding" of the upper triads of oxygen atoms (O31, O32, and O4) as a rigid group parallel to the b axis ($2M_1$ setting) and a "sliding" of the lower triads of symmetrically equivalent oxygen atoms in the opposite direction (Fig. 4); the z coordinates of these atoms do not change significantly as a result of this deformation.[4]

The deformation of the $2M_1$ octahedra described above causes four of the twelve $M1$–O and $M2$–O bond distances to become shorter, four to become longer, and four to remain almost the same relative to the equivalent bond distances in the $1M$ structure. Also, four of the six edges shared between octahedra change in the $2M_1$ form with respect to those of the $1M$ structure type (Fig. 4, Table 7): two become shorter (O4–O4, O31–O32), two become longer

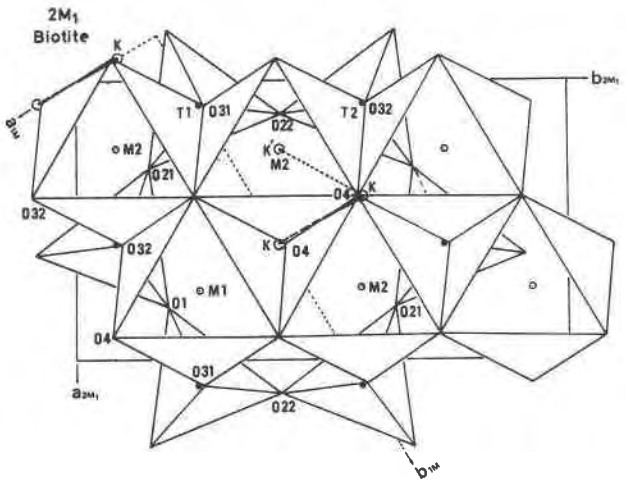

FIG. 1. The structure of $2M_1$ biotite from Ruiz Peak, New Mexico, projected on (001). The tetrahedral ring can be seen below the octahedral layer. Oxygen atoms are at the apices of the polyhedra. Cations are shown as circles. The K–K stacking vectors are shown as dashed lines. The potassium atom designated K′ is in the unit layer above the one shown. The $2M_1$ axial setting is shown as solid lines, the $1M$ setting as dashed lines.

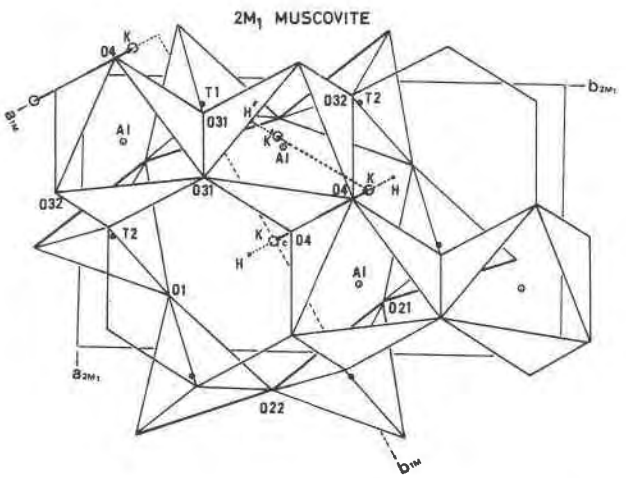

FIG. 2. The structure of $2M_1$ muscovite (Rothbauer, 1971). Notation as given in Figure 1. The hydrogen atom positions determined by neutron diffraction are shown as small solid circles. Note that the potassium positions (large open circles) are shifted slightly from the centers of the tetrahedral rings (c). K′ and H′ denote atoms in the unit layer above the one shown.

[4] In the $2M_1$ setting, this octahedral deformation is reflected only by a change in the y parameters of O3 and O4; in the $1M$ setting, it is reflected by a change in both x and y (Table 5a, Fig. 4).

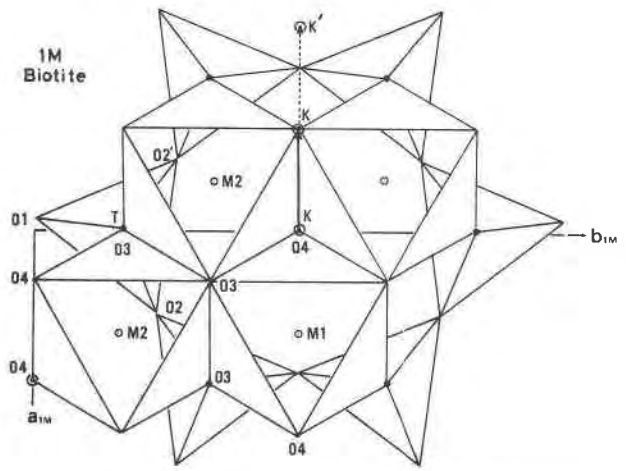

FIG. 3. The structure of 1*M* biotite from Ruiz Peak, New Mexico, projected on(001). Notation as given in Figure 1.

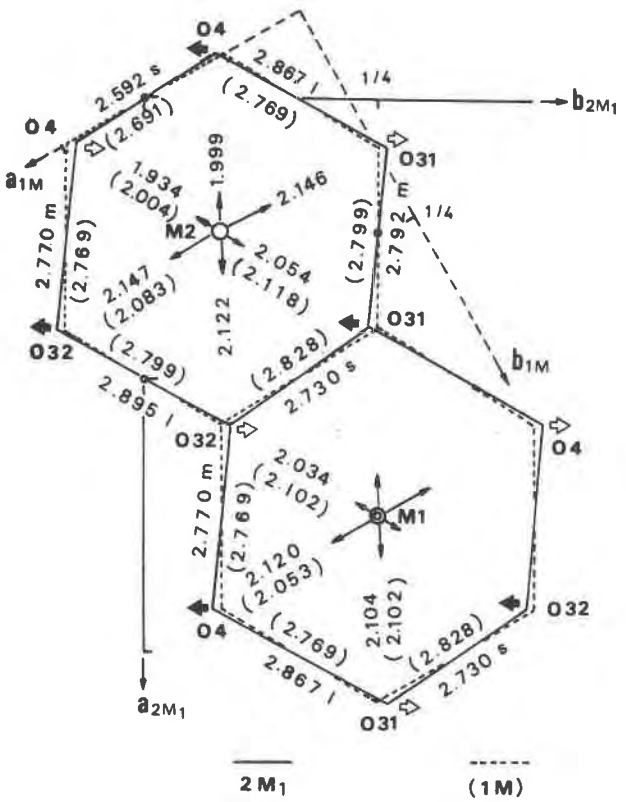

FIG. 4. Projection onto (001) of the *M*1 and *M*2 octahedral edges of the 1*M* (dashed lines) and $2M_1$ (solid lines) biotite structures. The metal–oxygen and oxygen–oxygen bond lengths are given, with those of the 1*M* polytype enclosed in parentheses. Explanation of the letters *m*, *s* and *l* is given in the text. Distortion of the $2M_1$ octahedra with respect to those of the 1*M* form is depicted with arrows, which indicate the relative displacement of the O3 and O4 oxygen atoms in the $\pm b$ direction.

(O31–O4, O32–O32), and two remain about the same (O31–O31, O32–O4). If we designate the shared edges of the *M*2 octahedra of the 1*M* form as *m-m-m-m-m-m* (observed in a clockwise sequence from the upper left of Fig. 4), the sequence of shared edges of the *M*2 octahedra of the $2M_1$ form becomes *s-l-m-s-l-m*, where *l* indicates a lengthened edge and *s* a shortened edge relative to the *m* edges of the 1*M* polytype. The sequence of these shared edges is *s-l-s-l-s-l* in the $2M_1$ muscovite structure. The unshared octahedral edges have the same lengths in the 1*M* and $2M_1$ biotites (Table 7).

The O3 oxygens of the octahedra are also the "apical" oxygens of the tetrahedra. In both the 1*M* and $2M_1$ biotites, the bases of the tetrahedra are nearly parallel to (001). In the (001) projection of the 1*M* biotite structure (Fig. 3), the tetrahedral cations lie just below the O3 apical oxygen atoms. In the projection of the $2M_1$ biotite structure (Fig. 1), however, the apical oxygens O31 and O32 are displaced away from *T*1 and *T*2, respectively. This shifting of O31 and O32 parallel to *b* causes a shortening of the O31–O22 distance and a lengthening of the O32–O22 distance relative to that found in the 1*M* structure (Table 6).

In the $2M_1$ muscovite structure (Fig. 2), the mode of deformation of the octahedral sheets is quite different from that found in the $2M_1$ biotite. The (001) projections of the octahedral edges O31–O31 and O32–O4 are parallel to *a* in $2M_1$ muscovite, whereas in $2M_1$ biotite they are not. In $2M_1$ biotite, the octahedral edges O32–O31 and O31–O4 are parallel to *b*, whereas in $2M_1$ muscovite they are not. The pseudo mirror planes[5] of the unit-layers are essentially retained in the $2M_1$ muscovite structure; in $2M_1$ biotite, they are not.

The structure of the tetrahedral sheet of $2M_1$ muscovite is also quite different from that found in $2M_1$ biotite. In muscovite, the oxygens (O1) are shifted towards the vacant octahedral sites by 0.4 Å, causing a distinct tilting of the tetrahedron. In $2M_1$ biotite, the tetrahedra remain essentially untilted.

Orientation of the O4–H Groups

Neutron diffraction study of a 1*M* phlogopite (Joswig, 1972) shows that the axis of the O4–H bond is normal to the unit-layer, the hydrogen atoms being positioned exactly above (or below) the O4 oxygens.

[5] The pseudo mirror planes include the O4–O4 octahedral shared edges and are perpendicular to the *b* axis of the unit layer in the 1*M* setting.

The potassium atoms lie immediately above (or below) the hydrogen atoms. We assume that the orientation of the O4–H vector in the Ruiz $1M$ biotite is the same as that found in $1M$ phlogopite.

The hydrogen position of $2M_1$ muscovite has also been accurately determined by neutron diffraction (Rothbauer, 1971). It was found that the O4–H vectors are inclined toward the vacant octahedral site ($M1$) and that the potassium atoms do not lie directly above (or below) the O4 and H atoms (Fig. 2) as they do in the $1M$ phlogopite structure. Also, the centers of the (Si_6O_{18}) ditrigonal rings are displaced from positions directly above (or below) the O4 oxygens. The O4–H, K–O4, and O4–O4 vectors, however, all lie within the pseudo-mirror plane of the unit layer (Fig. 2).

The $2M_1$ biotite structure possesses the same $\pm 120°$ stacking sequence as found in $2M_1$ muscovite; however, the potassium atoms do not lie within the pseudo mirror planes as found in muscovite but are displaced along a line parallel to the b direction ($2M_1$ setting, Fig. 1). This displacement of the potassium atoms and the "sliding" of the upper and lower triads of oxygen atoms of the octahedral layer along the $\pm b$ direction reduces the symmetry of the unit layer from the ideal $C2/m$ to $C\bar{1}$. This is in marked contrast to the unit layers of muscovite which to good approximation retain the ideal $C2/m$ symmetry. Note the pseudo-mirror plane oriented along an O1–O4 vector and perpendicular to b_{1M} of the muscovite structure depicted in Figure 2.

Our X-ray data do not give us any direct information on the position of the hydrogen atom in the $2M_1$ biotite structure. From the position of the potassium atoms and octahedral cations, however, we predict that the axis of the O4–H bond will be tilted away from a perpendicular to the unit layer and in a direction away from the potassium atom and in a plane nearly parallel to the b axis of the $2M_1$ unit cell. The vectors between K–H, H–O4, O4–O4, and K–K of a unit layer all lie within the mirror planes and pseudo-mirror planes of $1M$ biotite and $2M_1$ muscovite, respectively. The O4–O4 and K–K vectors in the $2M_1$ biotite structure do not lie within such a plane. When viewed in the (001) projection (Fig. 1), the O4–O4 vector is rotated counterclockwise with respect to the K–K vector.

Biotite Polytypism

Unit-Layer Structures

The structural differences between the unit layers of the $1M$ and $2M_1$ biotites studied here would suggest that these two polytypes have different fields of stability. Since we cannot demonstrate that the structural differences are caused by differences in chemical composition or differences in temperature and pressure of crystallization, we propose that they are caused by strain introduced by the geometrical and atomic restraints that one unit layer places upon the adjacent unit layers.

In the biotite series, individual layers can superimpose upon one another in three ways such that adjacent layers are related by a relative rotation about c^* of 0°, 120°, or −120°.[6] If we assume the structure of any particular unit-layer of a sequence is influenced only by the orientation of the layers immediately above and below, there are only four possible basic structures for a unit layer. These four types of layers are positioned in the middle of four different three-layer packets. The relative orientation of the three layers within these packets is defined by the vector stacking symbols [00], [02], [$2\bar{2}$], and [22], where: $0 = 0°$, $2 = 120°$, $\bar{2} = -120°$, and the first and last numbers within the bracket refer, respectively, to the rotation of the first relative to the second, and the second relative to the third layer of the packet.[7] We designate these four kinds of unit-layers as type [00], [02], [$2\bar{2}$], and [22]. Mica polytypes of the form $1M$[0], $2M_1$ [$2\bar{2}$], $3T$[222], and $6T$[020202] contain only type [00], [$2\bar{2}$], [22], and [02] unit layers, respectively.

The more complex Ruiz polytypes contain more than one type of unit layer; for example, the $3Tc_1$ [$02\bar{2}$] form contains [02] and [$2\bar{2}$] type layers and the $4M_2$ [2220] form contains [22] and [02] type layers. The Ruiz biotite $8Tc_{12}$ [$000\bar{2}\bar{2}02$] contains all four types of three-layer packets, which appear in the sequence: [00], [00], [02], [$2\bar{2}$], [$\bar{2}\bar{2}$], [$\bar{2}0$], [02], and [20]. This polytype, thus, theoretically, possesses all four types of unit layers within the unit cell. It would be informative to undertake a very careful crystal structure analysis of polytypes such as these to further delineate the effect of first (and second) nearest-neighbor layers on the structure of any particular unit layer.

Primary Platelet Growth

Baronnet (1972, 1973, 1974), from his studies of synthetic micas, proposes that mica crystal growth

[6] In most lithium-free trioctahedral micas relative layer rotations of 60°, 180°, and −60° are not permitted because of the presence of pseudo-trigonal symmetry at the layer interfaces.

[7] The vector stacking symbols (Ross *et al*, 1966) for the $1M$ and $2M_1$ polytypes are $1M$[0] and $2M_1$[$2\bar{2}$], respectively. Note that the stacking sequences [02] = [$0\bar{2}$] = [20] = [$\bar{2}0$], [22] = [$\bar{2}\bar{2}$], and [$2\bar{2}$] = [$\bar{2}2$].

starts as a simple nucleation of one layer upon another. If there exists in the Ruiz lava biotite nuclei one unit-layer thick, a second layer may nucleate upon the first in one of two ways: (1) with a relative layer rotation of 0° to initiate a $1M$ stacking sequence, and (2) with a relative layer rotation of 120° (or −120°) to initiate a $2M_1$ stacking sequence. In the Ruiz sample these two sequences appear to be equally probable, for about one-third of the crystals examined are $1M$ and one-third $2M_1$. Once a stacking sequence has started, we predict that the atomic and geometric constraints at the interlayer interface will distort the unit layers in different ways depending upon whether the sequence is of the $1M$ or $2M_1$ type. Further, we suggest that these interlayer constraints will tend to propagate an ordered sequence of layers, producing the basic $1M[0]$ or $2M_1[2\bar{2}]$ stacking arrangements within the primary platelet.

Occasionally, a unit layer will nucleate on a growing platelet in a "faulted" position with respect to the ordered $1M$ or $2M_1$ sequence, giving rise to unit layers of the type [02] or [22]. Continued ordered crystal growth of platelets containing only type [02] or [22] unit layers would produce a $6T[020202]$ or $3T[222]$ polytype. No $6T$ mica, nor any related to it, have been reported, but a number of polytypes closely related to the $3T$ form[8] have been found in the Ruiz specimen. It would appear from our present knowledge of the Ruiz biotites, that interlayer structural control during the initial stages of platelet growth is very strong for ordered $1M[0]$ and $2M_1[2\bar{2}]$ sequences, moderate for the $3T[222]$ sequence, and weak or nonexistent for the $6T[020202]$ sequence.

Spiral Growth

Baronnet has also shown that mica platelets once formed by nucleation of one layer upon another will often continue their growth by the Frank spiral mechanism through the introduction of a screw dislocation. The screw dislocation perhaps arises by an edgewise encounter of dendritic arms of a single crystal platelet.

In an elegant theoretical treatment of mica polytypism Baronnet (1975) considered the relationship between: (1) the layer sequence of the primary platelet, (2) the layer sequence within the spiral steps which are introduced above and below the platelet by a screw dislocation, and (3) the type of polytype generated by subsequent spiral crystal growth. The exact sequence of unit layers within the steps define the polytype. Primary platelets with unit layers in an ordered $1M$ sequence can develop only the $1M[0]$ form through spiral growth. Primary platelets with unit layers in an ordered $2M_1$ sequence develop by spiral growth polytypes of the form $1M[0]$, $2M_1[2\bar{2}]$, $3Tc[2\bar{2}0]$, $5Tc[(2\bar{2})_20]$, ... , $(2n+1)Tc[(2\bar{2})_n0]$, depending upon the number of unit layers within the dislocation steps and within the primary platelet.[9] Polytypes of the series $(n+1)Tc[(2\bar{2})_n0]$ have not yet been found in the Ruiz specimen but have been reported in synthetic muscovites by Baronnet, Amouric, and Chabot (in preparation).

Polytypes forming from a platelet having only type [22] unit layers can form three different polytypic series depending upon whether the dislocation step is 3 mod 3, 4 mod 3, or 5 mod 3 unit layers in height. These three types of steps form, respectively, the series $3T[222]$, $(3n+1)M[(222)_n0]$, and $(3n+2)M[(222)_n2\bar{2}]$. The latter two series are represented by the Ruiz polytypes $4M_2[2220]$, $8M_8[(222)_22\bar{2}]$, and $11M_1[(222)_32\bar{2}]$. Another important polytypic series found in the Ruiz specimen, as well as in other types of micas, has the form $(n+2)Tc[(0)_n2\bar{2}]$. Examples have been reported with $n = 1, 2, 6, 7, 12$, and 21 (Baronnet, 1975, Table 7). Such polytypes can originate from a primary platelet that has a dislocation step of $(n+2)$ layers and possesses a single "faulted" unit layer of the $[2\bar{2}]$ type.

Much more complex polytypes can arise if the primary platelet does not possess a simple ordered sequence of layers. Also, if the exposed upper and lower steps contain different stacking sequences, two different polytypes can form in one crystal. For example, consider a six-layer mica platelet with a layer stacking sequence $[020\bar{2}\bar{2}]$ and containing upper and lower steps with the sequences [02] and $[\bar{2}\bar{2}]$, respectively. Spiral growth will then generate the $3Tc[02\bar{2}]$ and $3T[\bar{2}\bar{2}\bar{2}]$ polytypes on the upper and lower surfaces, respectively. Baronnet's theory thus explains one possible origin of "coalescence" of polytypes.

Summary

1. The crystal structures of the unit layers of $1M$ and $2M_1$ biotite are significantly different and this difference does not appear to be related to any chemical differences between polytypes, nor to any differences in conditions of crystallization.

[8] A $3T[222]$ muscovite has been carefully studied by Güven and Burnham (1967). Detection of the $3T$ form is difficult, for its single crystal X-ray pattern is similar to the twinned $1M$ polytype and to the $3Tc_1$ form.

[9] The upper and lower spiral steps within an ordered platelet, which are of equal height and identical structure, generate identical polytypes on the (001) and $(00\bar{1})$ faces. The polytype pairs are, however, in 120° twinned relationship (twinning abbout [310] or $[3\bar{1}0]$) if the platelets are 2 mod 2 unit-layers thick.

2. The structure of the unit layer of the $2M_1$ polytype is characterized by a shifting, relative to the unit layer of the $1M$ polytype, of the upper and lower triads of octahedral oxygen atoms as a unit along the $\pm b$ directions. This causes a reduction of symmetry of the $2M_1$ unit layer from the ideal $C2/m$, as found in the $1M$ form, to $C\bar{1}$.

3. It is proposed that the structure of a particular unit layer of a polytype is directly related to the atomic and geometric constraints imposed on it by the adjacent unit layers, the constraints varying with the relative orientation of the adjacent layers. Thus, the unit layer of $1M$ polytype with adjacent layers in 0° relative orientation has a structure different from that of the unit layer of the $2M_1$ polytype which has adjacent layers in ±120° relative orientation.

4. It is further proposed that once interlayer constraints form between adjacent layers these constraints will tend to control the orientation of the next nucleated layer so as to give an ordered stacking sequence, usually of the $1M$ or $2M_1$ type, more rarely the $3T$ type.

5. Once a sequence of layers has formed through layer-by-layer nucleation within a growing mica platelet, further crystal growth often occurs by means of a spiral growth mechanism, the polytypic form of the final crystal being controlled by the sequence of layers within the primary platelet and within the dislocation step.

Acknowledgments

We wish to thank Dr. David R. Wones (U. S. Geological Survey) for his collaboration in studies of the mica polytypes, Mr. L. B. Wiggins (U.S.G.S.) for making the electron microprobe analyses, Dr. Robin Brett (U.S.G.S.), Professor R. Sadanaga, and Professor Y. Takéuchi (University of Tokyo) for the interest given us during the course of this work, and Dr. Alain Baronnet for furnishing us with preprints of his mica studies.

The computations were performed both at the computer center of the NASA Manned Spacecraft Center and at the Computer Center of the University of Tokyo. Part of the work was carried out at the NASA Manned Spacecraft Center while H. Takeda was supported by a National Research Council Senior Resident Associateship.

References

BARONNET, A. (1972) Growth mechanisms and polytypism in synthetic hydroxyl-bearing phlogopite. *Am. Mineral.*, **26,** 1272–1293.

——— (1973) Sur les origines des dislocations vis et des spirales de croissance dans les micas. *J. Crystal Growth,* **19,** 193–198.

——— (1975) The growth aspect of polymorphism/polytypism in synthetic micas of petrological interest. *Fortschr. Mineral.* (in press).

——— (1975) Growth spirals and complex polytypism in micas I—polytypic structure generation. *Acta Crystallogr.* **A31,** 345–355.

BURNHAM, C. W. (1966) Computation of absorption correction and the significance of end effect. *Am. Mineral.* **51,** 159–167.

———, Y. OHASHI, S. S. HAFNER, AND D. VIRGO (1971) Cation distribution and atomic thermal vibrations in an iron-rich orthopyroxene. *Am. Mineral.* **56,** 850–876.

———, AND E. W. RADOSLOVICH (1964) Crystal structures of coexisting muscovite and paragonite. *Carnegie Inst. Wash. Year Book,* **63,** 232.

CROMER, D. T. (1965) Anomalous dispersion corrections computed from self-consistent field relativistic Dirac-Slater wave functions. *Acta Crystallogr.* **18,** 17–23.

———, AND J. B. MANN (1968) X-ray scattering factors computed from numerical Hartree-Fock wave functions. *Acta Crystallogr.* **A24,** 321–324.

DONNAY, G., J. D. H. DONNAY, AND H. TAKEDA (1964) Trioctahedral one-layer micas. II. Prediction of the structure from composition and cell dimensions. *Acta Crystallogr.* **17,** 1374–1381.

FINGER, L. W. (1969) Determination of cation distributions by least-squares refinement of single-crystal X-ray data. *Carnegie Inst. Wash. Year Book,* **67,** 216–217.

GIUSEPPETTI, G., AND C. TADINI (1972) The crystal structure of $2O$ brittle mica: anandite (abstr.). *Acta Crystallogr.* **A28,** S70–71.

GÜVEN, N., AND C. W. BURNHAM (1967) The crystal structure of $3T$ muscovite. *Z. Kristallogr.* **125,** 163–183.

JOSWIG, W. (1972) Neutronenbeugungsmessungen an einem $1M$-phlogopit. *Neues Jahrb. Mineral. Monatsh.* **1972,** 1–11.

RADOSLOVICH, E. W. (1960) The structure of muscovite, $KAl_2(Si_3Al)O_{10}(OH)_2$. *Acta Crystallogr.* **13,** 919–932.

ROSS, M., H. TAKEDA, AND D. R. WONES (1966) Mica polytypes: Systematic description and identification. *Science,* **151,** 191–193.

ROTHBAUER, VON R. (1971) Untersuchung eines $2M_1$-Muskovits mit neutronenstrahlen. *Neues Jahrb. Mineral. Monatsh.* **1971,** 143–154.

TAKEDA, H. (1971) An improvement on the geometrical model structure of trioctahedral micas (abstr.), *Geol. Soc. Am. Abstr. Programs,* **3,** 727–728.

———, AND C. W. BURNHAM (1969) Fluor-polylithionite: a lithium mica with nearly hexagonal $(Si_2O_5)^{2-}$ ring. *Mineral. J.* **6,** 102–109.

———, N. HAGA, AND R. SADANAGA (1971) Structural investigation of polymorphic transition between $2M_2$-, $1M$- lepidolite, and $2M_1$ muscovite. *Mineral. J.* **6,** 203–215.

TAKÉUCHI, Y. (1964) Structures of brittle micas. *Proc. Nat. Conf. Clays Clay Minerals,* **13,** 1–25.

WONES, D. R. (1963) Physical properties of synthetic biotite on the join phlogopite–annite. *Am. Mineral.,* **48,** 1300–1321.

Manuscript received, August 13, 1974; accepted for publication, June 23, 1975.